Received 29 September 2024; Accepted 18 November 2024
https://doi.org/10.48612/letters/2024-4-399-405
https://elibrary.ru/nxjkbv

The simulation of the variation in the ultrasonic wave characteristics during the steel sample building by wire arc additive manufacturing

A. M. Ivanov†[1], S. P. Belyaev[1], V. V. Rubanik[2], N. N. Resnina[1], V. V. Rubanik jr.[2],
R. M. Bikbaev[1], I. V. Ponikarova[1], A. V. Sibirev[1]

†a.ivanov@spbu.ru

[1]Saint-Petersburg State University, Saint-Petersburg 199034, Russia
[2]Institute of Technical Acoustics of National Academy of Science of Belarus, Vitebsk 210009, Belarus

Abstract: The aim of the present paper is simulation of the ultrasonic wave propagation during sample building by additive manufacturing under ultrasonic assistance. The simulation was carried out using the explicit dynamics modulus of ANSYS. To find the mesh sizes for ANSYS simulation, the analytical solution of the wave equation was found using the dynamic Euler-Bernoulli beam equation. The mesh size was varied from 1 to 5 mm and the results were compared to Euler-Bernoulli solution. The best agreement between the solution and the simulation was found if mesh size was 2 mm. The ultrasonic wave propagation was simulated in the samples with a height varied from 6 to 60 mm. It was found that an increase in the sample height decreased the wave amplitude. If the sample height was larger than 30 mm, then the wave amplitude was different at various levels from the substrate. This occurred since the variation in geometric sizes and mass of the sample affected the planar second moment of area, cross-sectional area and boundary conditions that influenced the wave amplitude and number. In the samples with a height of 30 mm or less, the ultrasonic wave amplitude did not depend on the *y* position but it was different for various *z* position that might affect the mechanical properties. To confirm this assumption, two steel samples were manufactured without and under the ultrasonic assistance and the microhardness was measured in various cross-sections. It was found that the microhardness was the same in cross sections of the sample manufactured without ultrasonic assistance, and it was different in the sample produced under the ultrasonic assistance.

Keywords: ultrasonic vibrations, additive manufacturing, steel, simulation

Acknowledgments: *This work was supported by joint project of the St. Petersburg Science Foundation (grant number 23 RB-09-43) and the Belarus Republican Foundation for Fundamental Research (grant number T24СП6Г-008).*

1. Introduction

Nowadays the additive technologies (AT) are considered to be promising for manufacturing of complex-shaped parts of devices that significantly decrease their cost. The additive technologies may be divided to bed deposition (for instance, selective laser melting — SLM) or direct deposition (for example, wire-arc additive manufacturing — WAAM) [1–2]. Bed deposition technologies are usually used for the production of small metallic parts, for instance implants [3], whereas the direct deposition technologies are suitable for manufacturing of large metallic components [4]. Regardless of the type of additive technologies, the structure of manufactured components significantly differs from the one of samples produced by conventional ways. The main difference is the formation of columnar grains during solidification of layers, that leads to the formation of a [100] texture [1, 5–7]. As a result, the functional and mechanical properties show a strong anisotropy that significantly reduces the applications of the samples produced by AT. For instance, in [8–9], it was shown that the value of the shape memory effect in NiTi samples produced by WAAM was 2.5–3 times less than in NiTi samples produced by traditional techniques. This was attributed to the formation of [100] texture during manufacturing. At the same time, it is known that the [100] NiTi single crystals show the smallest recoverable strain [10]. Thus, the formation of [100] texture reduces the value of the shape memory effect in NiTi components produced by WAAM. The other reason is a small strain up to failure that is typical for coarse grain alloys.

The columnar grains form during solidification due to the epitaxial grain growth which is determined by the cooling rate and temperature gradient in the melt [1,11]. These parameters are hardly controlled during the WAAM, so the columnar grains appear in the samples as it is observed in cast alloys. To destroy the columnar grains in cast alloys, the thermo-mechanical treatment which includes the plastic deformation and post-deformation annealing is used. This approach is used for improvement of the structure of samples produced by WAAM [2,12–14]. It was shown that the hot rolling after the deposition of each layer or some layers allowed one to destroy the columnar grain structure. However, such a

technology requires the use of complex devices and it can be applied only for simple walls which are built perpendicular to the substrate.

The other way which affects the grain structure formation during the solidification of cast alloys is ultrasound-assisted crystallization or sonocrystallization [15–17]. In this case, ultrasonic vibrations are applied to the melt and prevent the dendrite formation and promote the appearance of equiaxed grains. Moreover, sonocrystallization leads to a more homogeneous distribution of precipitates in the matrix that improves the properties of alloys. There are many attempts to use ultrasonic vibrations during WAAM to control the samples structure [18–26]. All these attempts can be divided into two branches: the ultrasonic impact treatment (UIT) [18–21] and ultrasonic assisted treatment (UAT) [22–26]. UIT is used as post-processing treatment and it is close to the thermo-mechanical treatment mentioned above. UAT is used as in-process treatment where the ultrasonic vibrations are applied to the molten pool during deposition. This can be realized in moving regime, when an ultrasonic waveguide moves together with the heat source [22] or in a stationary regime when the ultrasonic vibrations are applied to the substrate on which a sample is built by WAAM [23–26]. The stationary regime does not require a specific equipment. However, in stationary regime, the ultrasonic amplitude is not constant over the length of a sample. Moreover, the geometry and mass of the sample may influence the parameters of ultrasonic vibrations such as the amplitude, wave number etc., during sample building. Thus, one can assume that during UAT, the ultrasonic wave parameters can be different in various parts of the sample that leads to the formation of different structures in the sample during WAAM. To find the effect of the ultrasonic vibration on the structure formation, the pressure field and flow field distributions in molten pool are simulated during the deposition of one layer [25–26]. However, the variation in the ultrasonic wave parameters in the samples has not been studied. The aim of the present paper is a simulation of the ultrasonic wave propagation in samples with various heights that corresponds to the building of a sample during additive manufacturing. To confirm the simulation results, two low-carbon steel samples were produced by WAAM without and with ultrasonic assistance and the structure and microhardness in various cross sections and along the sample heights were measured.

2. Simulation procedure

To simulate the ultrasonic vibrations in a sample deposited on a substrate by additive manufacturing, ANSYS Explicit Dynamics was used. The geometric models of a substrate with a size of 90×25×10 mm and deposited sample were created according to the real prototypes (Fig. 1). The *z*-axis was directed along the substrate length, *y*-axis was directed along the building direction, the *x*-axis was directed perpendicular to the *y* and *z*-axes. The sample layer was modeled as rectangular prism with sizes of 50×10×6 mm. To simulate the samples with various layers, the samples with various heights were used. So, the sample with two layers was simulated by a prism with a height of 12 mm; the sample with five layers as prism with a height of 30 mm, etc. The substrate and sample layers materials corresponded to an isotropic elastic material. The material constants were taken for low-carbon steel and are presented in Table 1. Connection between the sample and substrate was chosen to be rigid. Harmonic ultrasonic vibrations along the y axis with an amplitude of 9 μm and a frequency of 22 kHz were applied to a side surface of the hole in the substrate (shown by double red arrow in Fig. 1). The connection and friction between the hole surface and waveguide were not considered. All simulations were carried out in a stationary oscillations mode.

It is well known, that the less the mesh size, the closer the simulation results to analytical solution, but, the more the time of simulation [27]. To adjust the mesh size, the analytical solution of the wave propagation in the substrate was obtained. Beam vibrations are considered within the dynamic Euler-Bernoulli beam theory [28]. To find analytical solution, the following wave equation was solved:

$$EI_x v_y^{IV} + \rho S \ddot{v}_y = 0, \quad (1)$$

where v_y is the beam displacement in the *y* direction, *E* the Young's modulus, I_x the planar second moment of area, ρ the density and *S* the cross-sectional area.

Table 1. The material constants of low-carbon steel which were used for simulation.

Density	7850 kg/m^3
Young's modulus	160 GPa
Poisson ratio	0.3

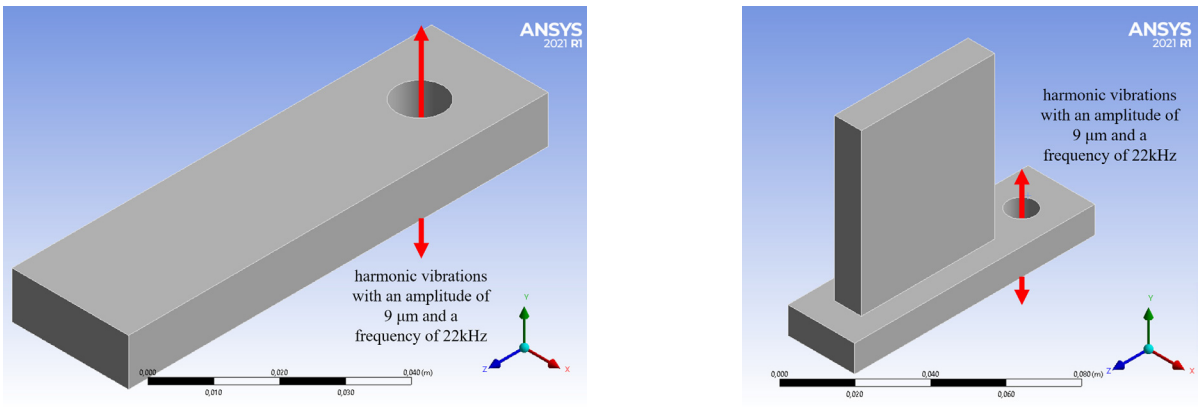

a b

Fig. 1. (Color online) Geometric models of substrate (a) and substrate with built sample (b) in the ANSYS.

The boundary conditions for the problem under consideration are written as follows:

$$\begin{cases} v_y(0,t) = A_0 \sin \omega t \\ v_y'(0,t) = 0 \\ M(l) = EIv_y''(l,t) = 0 \\ Q(l) = EIv_y'''(l,t) = 0 \end{cases} \quad (2)$$

where A_0 is the harmonic ultrasonic vibration amplitude (9 μm), t the time, l the length of beam and $\omega = 2\pi f$, where f is the ultrasonic vibration frequency (22 kHz).

A stationary solution should be found as $v_y(z,t) = U_y(z) \sin \omega t$. Then the deflection profile of the standing wave $U_y(z)$ must satisfy the following differential equation:

$$EI_x U_y^{IV} - \omega^2 \rho S U_y = 0 \quad (3)$$

In this case, the general solution is given as:

$$U_y(z) = A \cosh(\alpha z) + B \sh(\alpha z) + C \cos(\alpha z) + D \sin(\alpha z) \quad (4)$$

$$\alpha = \left(\frac{\rho S}{EI_x} \omega^2 \right)^{\frac{1}{4}}, \quad (5)$$

where α — wave number, A, B, C and D are constants which are defined according to boundary conditions (2). Using the data in Table 1 and the substrate geometrical sizes, the wave number α was calculated to be equal to 119 m^{-1}.

The simulations of the ultrasound vibrations in substrate were carried out with a mesh size of 1, 2, 3.3 and 5 mm. The dependencies of deflection amplitude (U_y) on z coordinate obtained for different mesh sizes are shown in Fig. 2 along with the analytical solution (black dash dot curve). It is seen, that the curves obtained during the simulation of the vibration in the sample with mesh size of 1 mm or 2 mm are close to the analytical curve. Therefore, the optimal mesh size was chosen to be 2 mm and used for simulation.

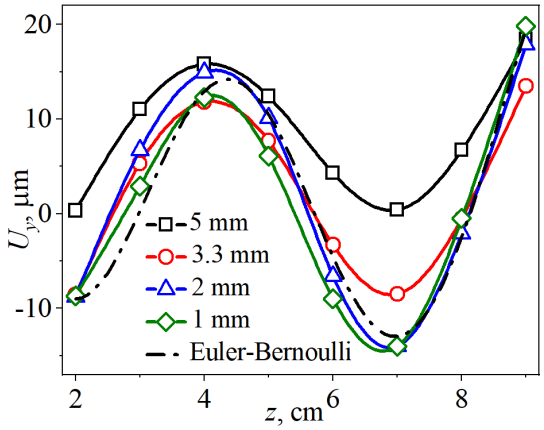

Fig. 2. (Color online) The dependencies of deflection amplitude (U_y) on z coordinate obtained on stationary vibrations of substrate with different mesh sizes.

3. Experimental procedure

The scheme of the substrate with a titanium ultrasonic waveguide as well as the image of experimental device and substrate with some deposited layers are shown in Fig. 3. Parameters of the WAAM manufacturing were as follows: scanning speed — 3 m/min, time gap between deposition of layers — 2 min, wire feedstock speed — 6 m/min, wire arc voltage — 4.5 V, number of layers — 7, substrate — low-carbon steel with a size of 90 mm × 25 mm × 10 mm, and the wire — low-carbon steel with a diameter of 1.2 mm. One sample was produced without ultrasonic assistance and its geometric size was 50 mm × 10 mm × 20 mm. The other sample was produced under ultrasonic assistance with a frequency of 22 kHz and amplitude of 15 μm. The ultrasonic vibrations were applied to the substrate during the whole process of sample deposition. After deposition, the sample had a size of 50 mm × 13 mm × 13 mm, hence the ultrasonic assistance increased the thickness of the sample.

Two cross sections were cut on distances of 12 and 25 mm from the free edge of the sample as shown in Fig. 4. Before the measurements, the cross-sections were polished by standard procedure when the abrasive paper was changed from 60 to 1200. The microhardness was measured by Vickers test (F=1 N, indentation time — 10 s) along the cross-section height and the average value was estimated using 30 points for each height.

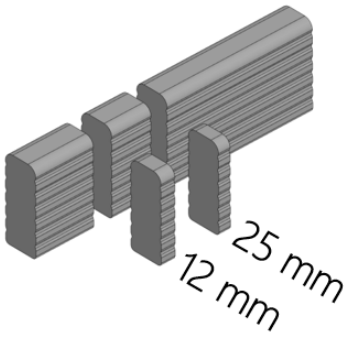

Fig. 4. The scheme of the cross-section cutting for the microhardness measurements.

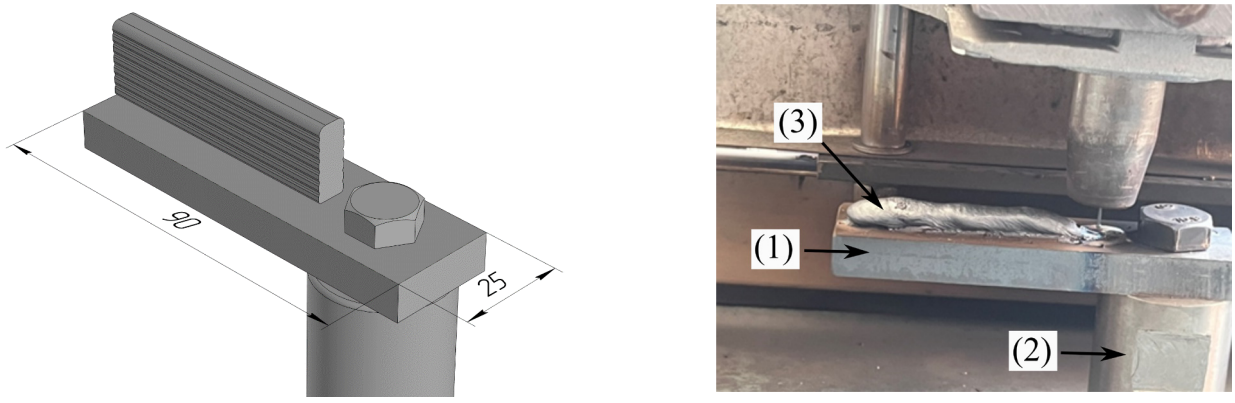

a b

Fig. 3. (Color online) The scheme (a) and image (b) of the steel substrate (1), titanium waveguide (2) and sample (3).

4. Results and discussion

Figure 5 shows a color map of the field of displacements in the y direction (U_y) in the substrate and samples with a height of 12, 30, and 60 mm (simulated 2, 5, and 10 layered samples). For convenience, these samples will be denoted as L2, L5 and L10. It is seen that in the L2 and L5 samples, U_y displacement changes different along the sample but is uniform along the sample height. (Fig. 5 a, b). In the L10 sample, the amplitude varies not only along the sample but also along the sample height (Fig. 5 c).

To analyse the variation in the ultrasonic vibration along the sample height, the $U_y(z)$ curves were found at different distances from the substrate (y) and plotted in Fig. 6. Zero "z" position corresponds to the edge of the hole. Zero "y" position shows the interface between the first layer and the substrate. It is seen that in L2 and L5 samples, the $U_y(z)$ curves differ from each other only in the vicinity of the sample edges (Fig. 6 a, b) due to the edge effects which influence the wave distribution in the sample. The less the height of the samples, the less the edge effect. In the L10 sample, the $U_y(z)$ curves are different at various levels from the substrate (Fig. 6 c). Moreover, the amplitude of the ultrasonic wave decreases with the sample height. So, in the L2 sample, the maximum amplitude is 12 μm, while in the L10 sample – only 4.5 μm.

An increase in the number of layers leads to an increase in the sample height that increases planar second moment

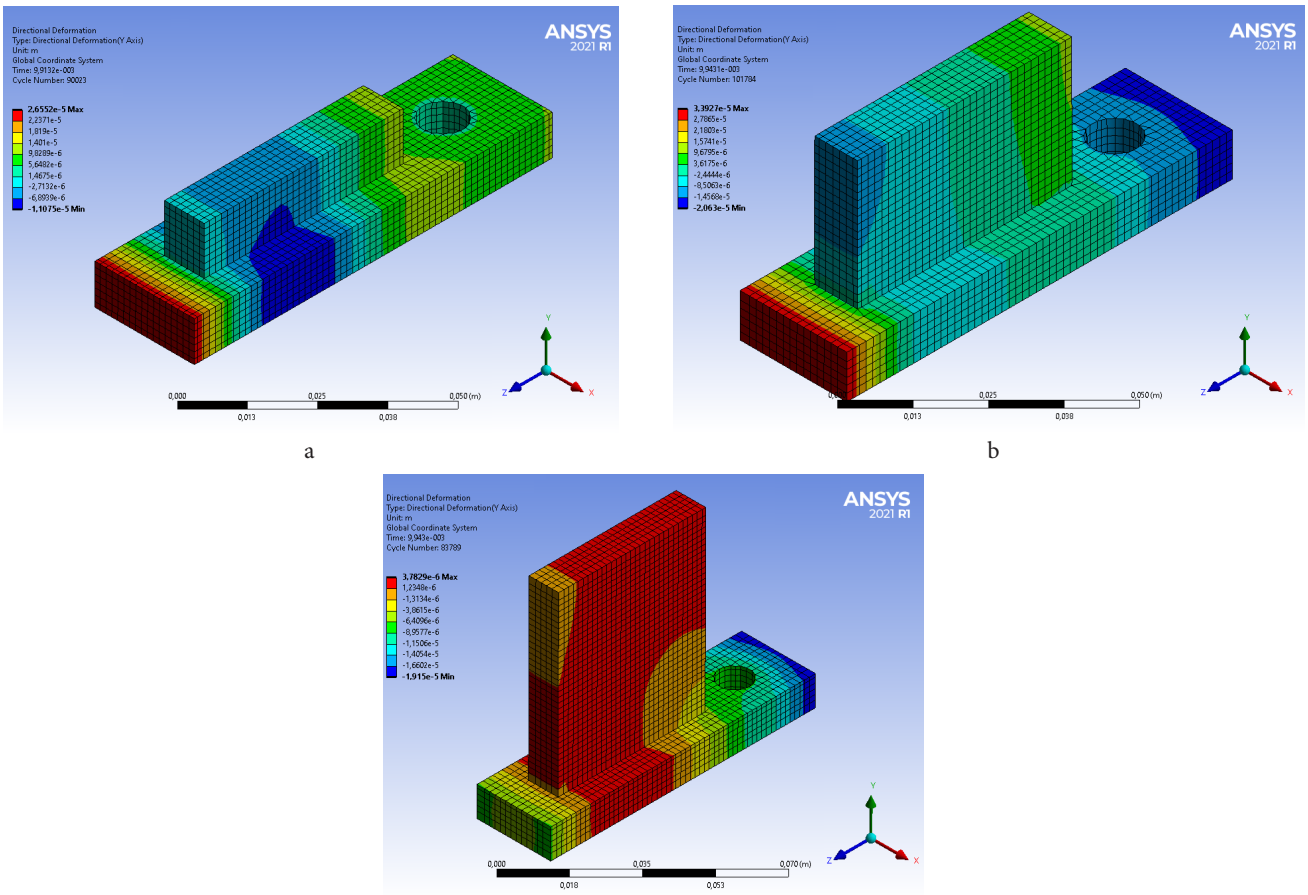

Fig. 5. (Color online) Colormap of displacement in the y-axis direction obtained on stationary vibration of substrate with 2 (a), 5 (b) and 10 (c) layers.

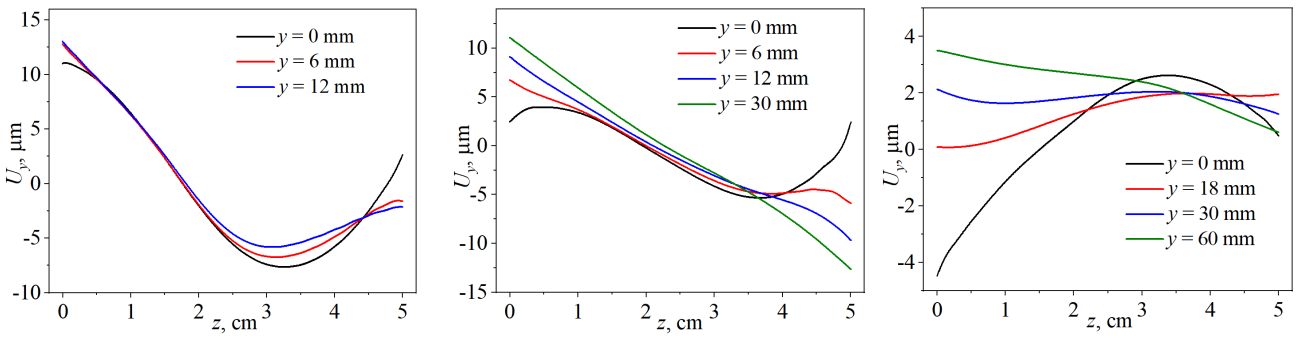

Fig. 6. (Color online) The $U_y(z)$ curves found at various distance (shown in legend) from the substrate in the L2 (a), L5 (b) and L10 (c) samples.

of area (I_x) and cross-sectional area (S). Both these values affect the wave number according to Eq. 5. With an increase in the sample height, the I_x and S values increase with various rates that results in a complex variation in the wave number. Moreover, the samples with various heights have different boundary conditions that affects the displacement and $U_y(z)$ curve.

During building of the sample by additive manufacturing, the number of layers increases that corresponds to an increase in the sample height in the simulation. To clarify the variation in the ultrasonic vibration parameters during sample building, $U_y(z)$ curves simulated at the same distance from the substrate (at the same y position) in samples with various heights were plotted and are presented in Fig. 7. It is clearly seen that an increase in sample height (in number of layers) decreases the oscillation amplitude. This means that during deposition of the first layer, the melt is subjected to vibrations with the maximum amplitude. During deposition of the next layers, the amplitude in the first, solid, layer decreases. Thus, the larger the height of a sample (number of layers), the less is the vibration amplitude in the first layer. The same is observed at any distance from the layer.

Thus, the results of the study show that the ultrasonic wave amplitude and the shape depend on the sample height. If the height of the sample is less than 30 mm, then the shape of the wave does not change. In this case, one may find the cross-sections with various amplitude. For instance, at $z = 30$ mm the amplitude is $|U_y| = 7.5$ μm, while at $z = 18$ mm, $|U_y|$ is equal to zero. If the ultrasonic vibration affects the sample structure, this influence can be different in various cross-sections. To clarify this assumption, two low-carbon steel samples with 7 layers were produced by WAAM without and under ultrasonic assistance (first sample was labeled as WAAM and the second samples as WAAM_US). In each sample, two cross-sections were cut and polished at a distance of 12 and 25 mm from the free edge, that corresponded to z values of 43 and 30 mm. The microhardness was found in the upper layers as an average value of 30 measurements. The study of the influence of the ultrasonic assistance during WAAM on the steel structure and properties is out of this study; hence they will be described in another paper.

The result obtained shows that columnar grains are observed in both samples in upper layers. However, their length in WAAM_US sample is significantly less than in WAAM sample (Fig. 8). Thus, the ultrasonic assistance during WAAM allowed obtaining a sample with smaller columnar grains. The microhardness values measured in various cross-sections of the WAAM sample are close to each other (184 ± 5 HV, Table 2). In WAAM_US sample, they are different that can be attributed to various wave parameters in different cross-sections.

Table 2. The microhardness measured in the columnar grains of the 7-layered steel samples manufactured by WAAM without or under ultrasonic assistance.

z, mm	Microhardness, HV	
	Without ultrasonic assistance	Under ultrasonic assistance
30	189	184
43.5	182	169

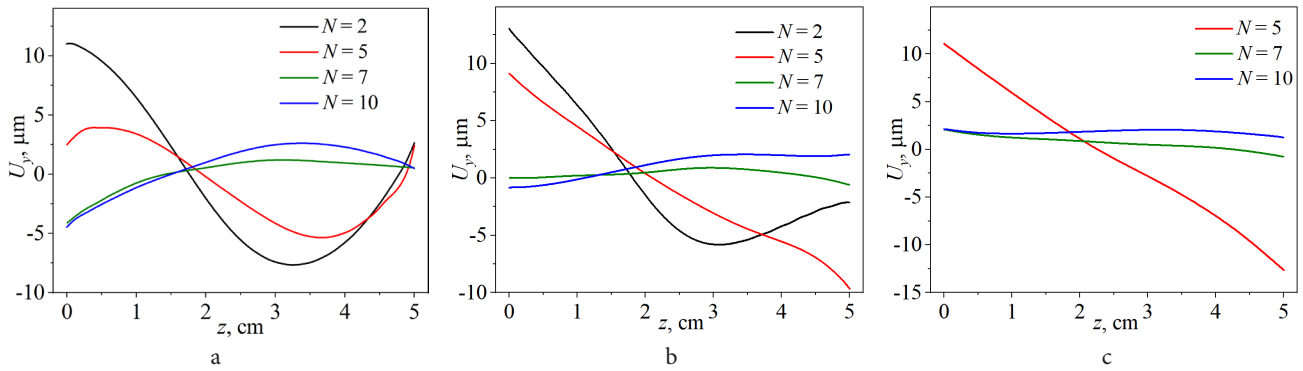

Fig. 7. (Color online) The $U_y(z)$ curves simulated at $y = 0$ (a), 12 (b) or 30 mm in the samples with various layer number (N).

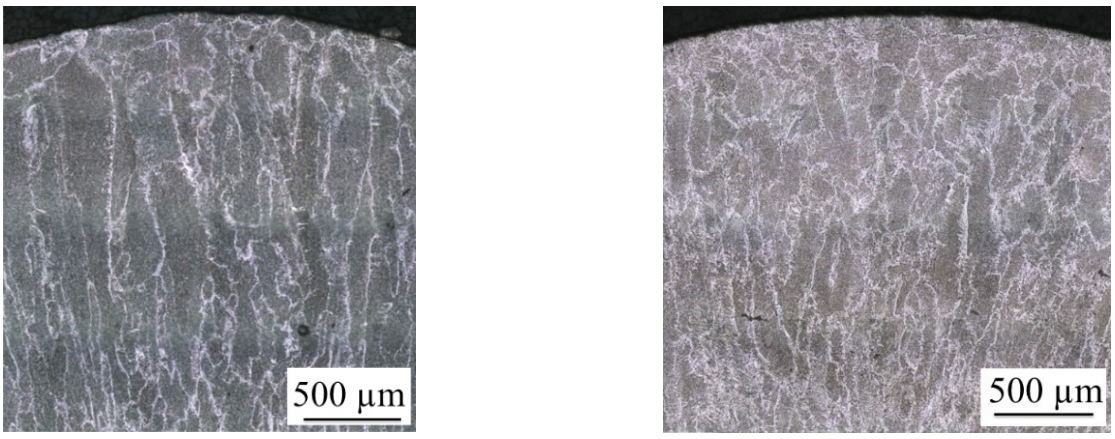

Fig. 8. Cross-section views of the 7-layered steel samples manufactured by WAAM without (a) or under ultrasonic assistance (b).

Thus, the results of the study show that that the ultrasonic assistance during additive manufacturing can be used as an effective tool for variation of the grain structure. At the same time, it is necessary to take into account that the ultrasonic wave parameters such as amplitude and wave number change during building of the sample due to the variation in geometrical sizes of the sample and its mass. An increase in the sample height decreases the ultrasonic amplitude. If the maximum height of the sample is less than 30 mm, then the amplitude decreases with an increase in the sample height but all parts of the same cross-section are subjected to the same vibrations. At the same time, the wave amplitude in various cross sections is different that can lead to various effects on the sample structure and properties. This is confirmed by the variation in the microhardness measured in various cross-sections in WAAM_US sample. If the maximum sample height is larger than 30 mm, then the wave amplitude is different even within one cross-section. Thus, the results of the study show that the samples with a height of 30 mm or less are more preferable for the production using WAAM under ultrasonic assistance because the wave propagation in them does not change with an increase in the distance from a substrate. However, this is valid only for given parameters of the ultrasonic assistance. Thus, it is necessary to study the influence of the power of ultrasonic vibrations on the wave propagation during building of the samples by WAAM that will be done out in future.

5. Conclusions

Main results may be formulated as followed:

1. An increase in the sample height during ultrasound-assisted WAAM decreases the wave amplitude. If the sample height is larger than 30 mm, then the wave amplitude depends on the distance from the substrate. The larger the distance, the less is the amplitude. This is due to the fact that a variation in geometric sizes and mass of the sample affects the planar second moment of area, cross-sectional area and boundary conditions that influence the wave amplitude and number.

2. In the samples with a height of 30 mm or less, the wave amplitude does not depend on the level from the substrate but it is different for various cross-sections.

3. Seven layered steel samples were produced by WAAM without and under ultrasonic assistance. No difference in the microhardness is found in various cross-sections of the sample produced by WAAM without ultrasonic vibrations. The microhardness is different in various cross-sections of the sample manufactured by WAAM under ultrasonic assistance that is caused by various ultrasonic amplitudes along the sample length.

References

1. T. DebRoy, H.L. Wei, J.S. Zuback, T. Mukherjee, J.W. Elmer, J.O. Milewski, A.M. Beese, A. Wilson-Heid, A. De, W. Zhang, Additive manufacturing of metallic components — Process, structure and properties, Progress in Materials Science 92 (2018) 112–224.
2. B. Wu, Z. Pan, D. Ding, D. Cuiuri, H. Li, J. Xu, J. Norrish, A review of the wire arc additive manufacturing of metals: properties, defects and quality improvement, J. Manuf. Process. 35 (2018) 127–139.
3. L.E. Murr, Metallurgy principles applied to powder bed fusion 3D printing/additive manufacturing of personalized and optimized metal and alloy biomedical implants: an overview, J Mater. Res. Technol. 9 (2020) 1087–1103.
4. J. Liu, Y. Xu, Y. Ge1, Z. Hou, S. Chen, Wire and arc additive manufacturing of metal components: a review of recent research developments, Int. J. Adv. Manuf. Technol. 111 (2020) 149–198.
5. G. Asala, A.K. Khan, J. Andersson, O.A. Ojo, Microstructural Analyses of ATI 718Plus Produced by Wire-ARC Additive Manufacturing Process, Metal. Mater. Trans. A, 48A (2017) 4211–4228.
6. S. Saedia, A.S. Turabia, M.T. Andani, N.S. Moghaddam, M. Elahinia, H.E. Karaca, Texture, aging, and superelasticity of selective laser melting fabricated Ni-rich NiTi alloys, Materials Science & Engineering A 686 (2017) 1–10.
7. J. Wang, Z. Pan, K. Carpenter, J. Han, Z. Wang and H. Li, Comparative study on crystallographic orientation, precipitation, phase transformation and mechanical response of Ni-rich NiTi alloy fabricated by WAAM at elevated substrate heating temperatures, Mater Sci Eng A., 800 (2021) 140307.
8. N. Resnina, I.A. Palani, S. Belyaev, S.S. M. Prabu, P. Liulchak, U. Karaseva, M. Manikandan, S. Jayachandran, V. Bryukhanova, A. Sahu, R. Bikbaev, Structure, martensitic transformations and mechanical behaviour of NiTi shape memory alloy produced by wire arc additive manufacturing J. Alloys Compd. 851 (2021) 156851.
9. N. Resnina, I.A. Palani, S. Belyaev, S. Singh, A. Kumar, R. Bikbaev, A. Sahu, Functional Properties of the Multilayer NiTi Alloy Produced by Wire Arc Additive Manufacturing, Shape Mem. Superelasticity 8 (2022) 5–15.
10. K. Gall, H. Sehitoglu, Y.I. Chumlyakov, I.V. Kireeva, Tension-compression asymmetry of the stress-strain response in aged single crystal and polycrystalline NiTi. Acta Mater. 47 (1999) 1203–1217.
11. F. Yan, W. Xiong, E.J. Faie, Grain Structure Control of Additively Manufactured Metallic Materials, Mater. 10 (2017) 1260.
12. F.W. Cipriano Farias, T.J. Gomes dos Santos, J.P. Oliveira, Directed energy deposition + mechanical interlayer deformation additive manufacturing: a state-of-the-art literature review, J. Adv. Manuf. Technol. 131 (2024) 999–1038.
13. J. Donoghue, A.A. Antonysamy, F. Martina, P.A. Colegrove, S.W. Williams, P.B. Prangnell, The effectiveness of combining rolling deformation with Wire-Arc Additive Manufacture on β-grain refinement and texture modification in Ti-6Al-4V, Mater. Charact. 114 (2016) 103–114.
14. G.I. Eskin, Influence of cavitation treatment of melts on the processes of nucleation and growth of crystals during solidification of ingots and castings from light alloys, Ultrasonics Sonochemistry 1 (1994) S59-S63.

15. M. D. Luque de Castro, F. Priego-Capote, Ultrasound-assisted crystallization (sonocrystallization), Ultrason. Sonochem. 14 (2007) 717 – 724.
16. V. S. Nalajala, V. S. Moholka, Investigations in the physical mechanism of sonocrystallization, Ultrasonics Sonochemistry 18 (2011) 345 – 355.
17. A. E. Davis, J. R. Honnige, F. Martina, P. B. Prangnel, Quantification of strain fields and grain refinement in Ti-6Al-4V inter-pass rolled wire-arc AM by EBSD misorientation analysis, Materials Characterization 170 (2020) 110673.
18. Y. Cao, Y. Zhang, W. Ming, W. He, J. Ma, Review: The Metal Additive-Manufacturing Technology of the Ultrasonic-AssistedWire-and-Arc Additive-Manufacturing Process, Metals 13 (2023) 398.
19. D. Yuan, S. Shao, C. Guo, F. Jiang J. Wang, Grain refining of Ti-6Al-4V alloy fabricated by laser and wire additive manufacturing assisted with ultrasonic vibration, Ultrasonics Sonochemistry 73 (2021) 105472.
20. C. Wang, Y. Li, W. Tian, J. Hu, B. Li, P. Li, W. Liao, Influence of ultrasonic impact treatment and working current on microstructure and mechanical properties of 2219 aluminium alloy wire arc additive manufacturing parts, J. Mater. Res. Technol. 21 (2022) 781 – 797.
21. V. K. Sahu, R. Biswal, A. E. Davis, X Chen, S. W. Williams, P. B. Prangnell, β-Grain refinement in WAAM Ti-6Al-4 V processed with inter-pass ultrasonic impact peening, MTLA 38 (2024) 102236.
22. T. Wang, X. Liu, M. Darnell, Ultrasonic effects with different vibration positions on gas tungsten arc wire additive manufactured aluminum nanocomposite, J. Manuf. Proces., 105 (2023) 359 – 369.
23. J. Zhang, Y. Xing, J. Zhang, J. Cao, F. Yang, X. Zhang, Effects of In-Process Ultrasonic Vibration on Weld Formation and Grain Size of Wire and Arc Additive Manufactured Parts, Mater. 15 (2022) 5168.
24. M. Zhang, B. Wang, X. Li, G. Jiao, X. Fang, K. Huang, Grain refinement of NiTi alloys during ultrasound-assisted wire-arc directed energy deposition, Virtual and Physical Prototyping, 19 (2024) e2289465.
25. F. Ji, X. Qin, Z. Hu, X. Xiong, M. Ni, M. Wu, Influence of ultrasonic vibration on molten pool behavior and deposition layer forming morphology for wire and arc additive manufacturing, Int. Commun. Heat Mass Transfer 130 (2022) 105789.
26. F. Ji, Z. Hu, X. Qin, F. Yin, M. Ni, X. Xiong, Grain refinement and mechanism of steel in ultrasound assisted wire and arc additive manufacturing, International Communications in Heat and Mass Transfer 143 (2023) 106724.
27. O. C. Zienkiewicz, R. L. Taylor, The Finite Element Method: Its Basis and Fundamentals, Butterworth-Heinemann publishing, 2013, 756 p.
28. S. M. Han, H. Benaroya, T. Wei, Dynamics of transversely vibrating beams using four engineering theories, J. Sound Vib. 225 (1999) 935 – 988.